Thrombogenic collagen-mimetic peptides: Self-assembly of triple helix-based fibrils driven by hydrophobic interactions

Mabel A. Cejas*, William A. Kinney*†, Cailin Chen*, Jeremy G. Vinter‡, Harold R. Almond, Jr.*, Karin M. Balss§, Cynthia A. Maryanoff§, Ute Schmidt¶, Michael Breslav*, Andrew Mahan*, Eilyn Lacy‖, and Bruce E. Maryanoff*†

*Research and Early Development, Johnson & Johnson Pharmaceutical Research & Development, Spring House, PA 19477-0776; ‡Cresset BioMolecular Discovery, Ltd., Welwyn Garden City, Hertfordshire AL7 3AX, United Kingdom; §Convergent Product Development, Cordis, a Johnson & Johnson Company, Spring House, PA 19477-0776; ¶WITec GmbH, D-89081 Ulm, Germany; and ‖Protein Engineering, Centocor Research and Development, Radnor, PA 19087-4517

Edited by M. Reza Ghadiri, The Scripps Research Institute, La Jolla, CA, and accepted by the Editorial Board April 3, 2008 (received for review January 11, 2008)

Collagens are integral structural proteins in animal tissues and play key functional roles in cellular modulation. We sought to discover collagen model peptides (CMPs) that would form triple helices and self-assemble into supramolecular fibrils exhibiting collagen-like biological activity without preorganizing the peptide chains by covalent linkages. This challenging objective was accomplished by placing aromatic groups on the ends of a representative 30-mer CMP, $(GPO)_{10}$, as with L-phenylalanine and L-pentafluorophenylalanine in 32-mer 1a. Computational studies on homologous 29-mers 1a′–d′ (one less GPO), as pairs of triple helices interacting head-to-tail, yielded stabilization energies in the order 1a′ > 1b′ > 1c′ > 1d′, supporting the hypothesis that hydrophobic aromatic groups can drive CMP self-assembly. Peptides 1a–d were studied comparatively relative to structural properties and ability to stimulate human platelets. Although each 32-mer formed stable triple helices (CD) spectroscopy, only 1a and 1b self-assembled into micrometer-scale fibrils. Light microscopy images for 1a depicted long collagen-like fibrils, whereas images for 1d did not. Atomic force microscopy topographical images indicated that 1a and 1b self-organize into microfibrillar species, whereas 1c and 1d do not. Peptides 1a and 1b induced the aggregation of human blood platelets with a potency similar to type I collagen, whereas 1c was much less effective, and 1d was inactive (EC_{50} potency: 1a/1b ≫ 1c > 1d). Thus, 1a and 1b spontaneously self-assemble into thrombogenic collagen-mimetic materials because of hydrophobic aromatic interactions provided by the special end-groups. These findings have important implications for the design of biofunctional CMPs.

biomaterial | platelets | structure–function | supramolecular triplex

The self-association of peptides and proteins into well ordered supramolecular structures is of pivotal importance in normal physiology and pathophysiology, such as in the assembly of collagen fibrils (1), actin filaments (2), and amyloid fibrils (3, 4). Collagens, which constitute a ubiquitous protein family in animals, contribute an essential matrix component to soft tissues and bones (5, 6). A structural hallmark of many collagens is a rope-like triple helix, the architecture of which derives from the interplay of three proline-rich polypeptide strands (e.g., two α1 and one α2 for type I collagen) (6–8). In the core domain of the triple helix, the amino acid sequence G-X-Y is repeated multiple times, and each glycine amide NH forms a hydrogen bond with the X-position amide carbonyl on an adjacent strand. The X- and Y-positions are often populated by L-proline and 4(*R*)-hydroxy-L-proline (O; Hyp), respectively, with the latter stabilizing the triple helix by stereoelectronic effects (9) and water-bridged hydrogen bonds (10).

To investigate collagen's structure and function, researchers have resorted to using synthetic collagen model peptides (CMPs) with the sequences $(GXY)_n$, where X and Y are natural or unnatural amino acids and n = 5–10 (11, 12). Analytical methods, such as x-ray crystallography, circular dichroism (CD) spectroscopy, and dynamic light scattering (DLS), have yielded structural information relevant to collagen mimicry (11, 12). However, much less attention has been directed to CMPs that manifest collagen-like biological properties. A challenge in this area is devising CMPs that spontaneously self-assemble into collagen-mimetic materials without the aid of covalent linkages (13, 14). After reviewing various structural concepts, we hypothesized that suitably disposed hydrophobic interactions may be applicable to this problem.

Self-assembly is a powerful technique for organizing molecular building blocks into complex structures (15) and aromatic groups can facilitate this process (16–18). For example, the Phe–Phe dipeptide motif in Alzheimer's disease β-amyloid protein was able to self-assemble into peptide-based nanotubes (19). In fact, aromatic residues play an important role in collagen self-assembly from the requirement of the telopeptide regions of collagen (20), especially the Tyr and Phe residues within the C-terminal chain (21). Thus, we pursued a strategy predicated on using hydrophobic amino acids as recognition elements, attached to the termini of a 30-mer CMP. The modified single strand should adopt a triple-helix structure and then, it was hoped, self-assemble with end-to-end stacking of triplex building blocks into supramolecular fibrils, by strictly noncovalent means. This approach proved to be successful, as observed in our preliminary work with 32-mer peptide **1a** (Fig. 1), which yielded a bioactive, collagen-like material (22). However, it is important to gain a better understanding of the scope and limitations of such CMP self-assembly, and to develop a correlation between structure and function. In this vein, we have now conducted experiments to compare four analogous 32-mer CMPs with different end-groups, **1a-d** (Fig. 1). Our studies establish the structural properties of these CMPs *vis-à-vis* their biological activity, in terms of thrombogenicity, and support the proposal

Author contributions: M.A.C., W.A.K., J.G.V., K.M.B., C.A.M., and B.E.M. designed research; M.A.C., C.C., J.G.V., H.R.A., K.M.B., U.S., M.B., A.M., and E.L. performed research; M.A.C., W.A.K., C.C., J.G.V., H.R.A., K.M.B., C.A.M., U.S., M.B., A.M., E.L., and B.E.M. analyzed data; and W.A.K. and B.E.M. wrote the paper.

Conflict of interest statement: M.A.C, W.A.K., C.C., J.G.V., H.R.A., K.M.B., C.A.M, U.S., M.B., A.M. E.L., and B.E.M. conducted the studies described herein while employed by a commercial enterprise.

This article is a PNAS Direct Submission. M.R.G. is a guest editor invited by the Editorial Board.

†To whom correspondence may be addressed. E-mail: wak@pei3.com or bmaryano@prdus.jnj.com.

This article contains supporting information online at www.pnas.org/cgi/content/full/0800291105/DCSupplemental.

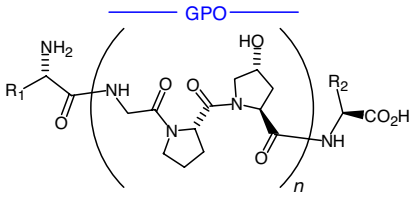

1a: $n = 10$; $R_1 = (C_6F_5)CH_2$-, $R_2 = PhCH_2$-
1b: $n = 10$; R_1, $R_2 = PhCH_2$-
1c: $n = 10$; $R_1 = Me_2CHCH_2$-, $R_2 = PhCH_2$-
1d: $n = 10$; R_1, $R_2 = H$
2: $n = 5$; $R_1 = (C_6F_5)CH_2$-, $R_2 = PhCH_2$-

Fig. 1. Structures of **1a–d** and **2**.

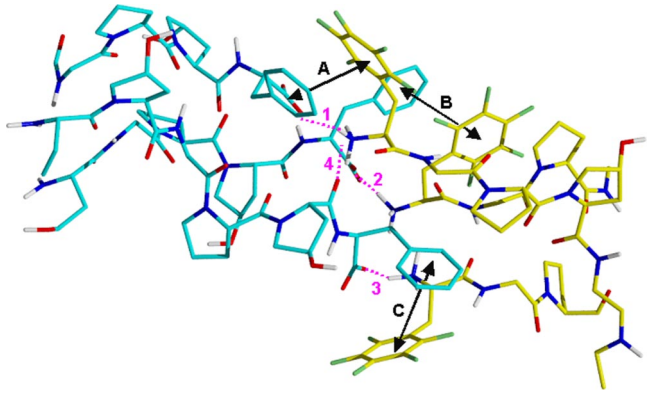

Fig. 2. Interface from energy-minimized structure of triple-helical, head-to-tail homodimer $(\mathbf{1a}')_3/(\mathbf{1a}')_3$ (one blue, one yellow; standard atom-coloring scheme for N, O, F, and H) showing three aromatic stacking interactions (black double-headed arrows; A–C) and three salt bridges with hydrogen bonds (magenta dotted lines; 1–3), each involving an ammonium group (NH_3^+) and a carboxylate group (CO_2^-). The H-bond between an ammonium and a backbone carbonyl is also shown (magenta dotted line; 4).

that specific hydrophobic interactions can drive the self-assembly of collagen-related peptides into functional, supramolecular, fibrillar materials.

Results

Design of Collagen-Model Peptides. To ensure a stable triple helix at 25–37°C, we considered a CMP core structure with 30 amino acids in the chain, i.e., $(GPO)_{10}$. For suitable hydrophobic interactions to facilitate self-assembly into supramolecular fibrils, we would add aromatic subunits onto the N and C termini. Phenyl and pentafluorophenyl groups emerged as good candidates because of strong noncovalent aromatic-stacking interactions between benzene and hexafluorobenzene (23, 24). Thus, we decided to append L-pentafluorophenylalanine (F_5-Phe) and L-phenylalanine (F) onto the ends of 30-mer $(GPO)_{10}$, as in 32-mer **1a** (Fig. 1). Peptides **1b** (Phe/Phe pair) and **1c** (Phe/Leu pair) were meant to test the adequacy of other hydrophobic interactions: a weaker aromatic-aromatic interaction and an aromatic-aliphatic interaction. The end-groups plus the interface between juxtaposed, head-to-tail triplexes subtends the space of one GPO to provide a continuous GPO-repeat distance in an axial alignment of triple-helical building blocks. We speculated that ordered hydrophobic interactions ought to encourage propagation of 32-mer building blocks, by end-to-end stacking, into lengthy strands akin to the fibrils of certain native collagens (5, 6). This hypothesis was first tested theoretically via molecular mechanics calculations on 29-mer homologues of **1a–c** with one less GPO ($n = 9$; **1a′–c′**) as head-to-tail triple-helical homodimers with three π-stacking interactions and one salt bridge (22). We reexamined the interface of the triplex homodimer of **1a′** $[(\mathbf{1a}')_3/(\mathbf{1a}')_3]$ and concluded that three salt bridges and three π-stacking interactions could be established in the context of a "six-point model." Energy minimization of this structurally revised homodimer, $(\mathbf{1a}')_3/(\mathbf{1a}')_3$, with an extended electron distribution (XED) force field (25, 26), afforded the energy for dimer interaction (see *Materials and Methods*). The six key interactions were retained and the total binding energy (*in vacuo*; enthalpic) was calculated to be −83.5 kcal/mol [Fig. 2, supporting information (SI) Fig. S1, and Table S1]. The pre-XED model for $(\mathbf{1a}')_3/(\mathbf{1a}')_3$ was used to construct starting homodimers for **1b′–d′**, and their binding energies (kcal/mol) were computed (XED): **1b′**, −70.4; **1c′**, −58.9; **1d′**, −43.8. Thus, our calculated stabilization energies for head-to-tail, triplex homodimers of **1a′–d′** are in the order **1a′** > **1b′** > **1c′** > **1d′**, which suggests a marked advantage for self-assembly of 32-mer **1a** into ordered molecular aggregates, such as fibrils.

Synthesis and Characterization of CMPs. Peptides **1b–d** were synthesized and purified for comparison with **1a**, in experimental studies geared to establish (1) the relationship between hydrophobic end-group interactions and the propensity for self-assembly, and (2) the structural requirements for biological activity in terms of thrombogenicity. As a control, we prepared and used 17-mer $(F_5\text{-Phe})\text{-}(GPO)_5\text{-Phe}$ (**2**) (Fig. 1) (27). Peptides **1a–d** and **2**, from solid-phase synthesis, were purified by reversed-phase (RP) HPLC on a heated column (see *Materials and Methods*). Their identities were confirmed by MALDI-TOF MS and amino acid analysis.

Peptides **1a–d** and **2** were analyzed by CD spectroscopy to determine triple-helical content. After incubation at 4°C for 24 h in water, **1a–d** exhibited a positive peak near 225 nm (Fig. 3*A*), which is characteristic for collagen triple helices, but **2** showed a much weaker positive peak at 222 nm. Thermal stability of the triple helices for **1a–d** was evaluated by monitoring the 225-nm signal with increasing the temperature (Fig. 3*B*). The melting

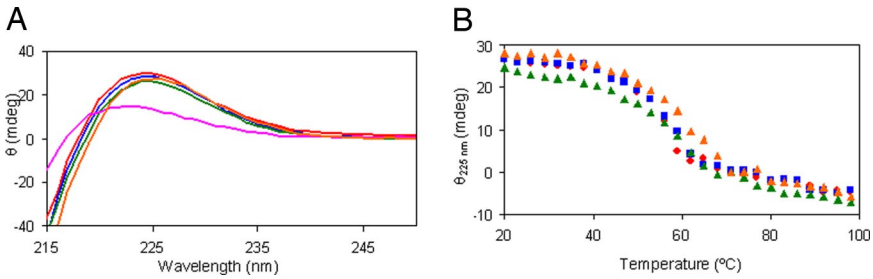

Fig. 3. CD spectral data. (*A*) CD curves for **1a** (red), **1b** (blue), **1c** (green), **1d** (orange), and **2** (pink). (*B*) CD melting curves for **1a** (red), **1b** (blue), **1c** (green), and **1d** (orange).

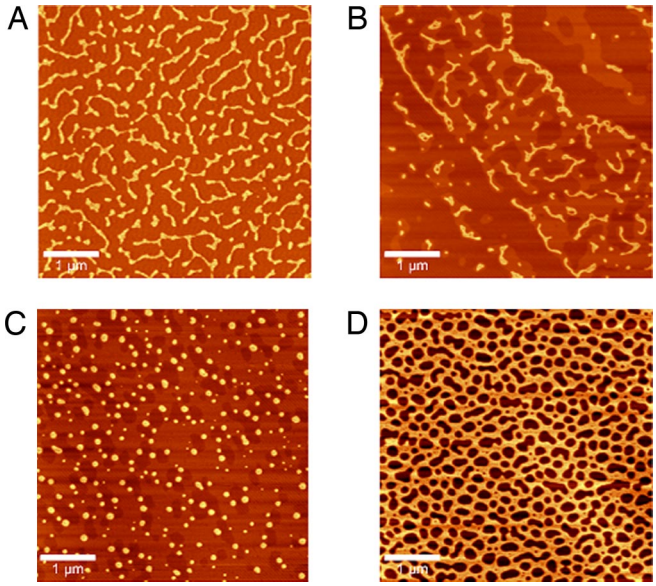

Fig. 4. AC-AFM topography images for **1a** (*A*), **1b** (*B*), **1c** (*C*), and **1d** (*D*) from incubated aqueous solutions (0.1 mg/ml) deposited onto freshly cleaved mica. (Scale bars, 1 μm.)

temperatures (T_m) for **1a–d** were in the range of 56–62°C, but the melting curve for **2** had no clear transition (Fig. S2).

Self-Assembly of CMPs. A crucial aspect was assessment of the triple-helical CMPs for their ability to self-assemble into supramolecular materials. In an earlier study (22), we found that **1a** forms high-order aggregates of micrometer-size by using DLS, whereas 31-mer Ac(GPO)$_{10}$G (**3**), which lacks special end-groups, does not. Thus, we sought to analyze 32-mers **1a–d** comparatively by DLS, but attempts to differentiate the peptides were unsuccessful, possibly related to inherent variability in this type of measurement. However, by using light microscopy to compare **1a**, **1d**, and type I collagen (0.05 mg/ml in water), we observed >100-μm fibrils for **1a** that resembled collagen fibrils but only observed large globular conglomerates for **1d** (Fig. S3).

Atomic force microscopy (AFM) proved to be a very effective method for imaging CMP morphology (*SI Text*, *AFM Background*). Aqueous solutions of **1a–d** were heated to 73°C for 10 min to facilitate disaggregation, filtered to remove any aggregated material, diluted, and let stand ("incubated") for 24 h at 23°C. A sample of each peptide was deposited onto freshly cleaved mica. Peptides **1a** and **1b** formed fibrous aggregates, with lengths ranging from 0.5 to 5 μm (Fig. 4 *A* and *B*). High-resolution images of **1a** and **1b** revealed a periodicity pattern (*D*) of ≈33 ± 3 nm (Fig. S4). At 0.1 mg/ml, **1a** and **1b** yielded a network of fibrillar material, including long fibrils (>5 μm) with branches, and smaller branched fibrils on closely packed tubular fibrils. By contrast, at 0.1 mg/ml (and 1.0 mg/ml), **1c** formed small spherical aggregates <0.5 μm in diameter, and **1d** wet the surface unevenly, forming sheets with irregular shaped holes (Fig. 4 *C* and *D*). Phase images for **1a–c** indicated that **1a** and **1b** are much stiffer, consistent with self-assembly of **1a** and **1b** into supramolecular fibrils (Fig. S5). AFM images of collagen showed μm-length fibrils with a periodic band gap of 62 ± 2 nm (Fig. S6) (28).

We made an unusual observation related to the self-assembly of **1a** in turbidity experiments with **1a** and (POG)$_{10}$ (**4**) (29), which lacks special end-groups. Solutions of **1a** and **4** (PBS, 5 mg/ml) were heated at 80°C, filtered (0.45 μm), held at 45°C, and monitored at 313 nm for 0–85 min (Fig. S7). There was a marked increase in absorbance for **4** in this time period (29), but the absorbance for **1a** did not change. After aging at 23°C for 3 days, **4** gave a thick precipitate and **1a** gave fine particles. Intriguingly, light microscopy images of particles from **1a** showed millimeter-size objects in the form of an ordered hydrogel, with apparent periodic banding (Fig. 5), whereas **4** did not form such objects.

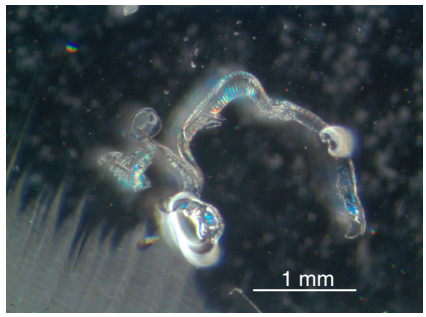

Fig. 5. Light microscopy image of a particle from self-assembly of **1a**. (Scale bar, 1 mm.)

Platelet Aggregation Studies. Circulating blood platelets adhere to exposed collagen in an injured vessel wall to prevent bleeding and promote tissue repair. This basic platelet function is mediated by the collagen receptor, glycoprotein VI (GP VI), which triggers intracellular signal transduction that activates the integrin GP IIb/IIIa and induces platelet aggregation (30). Platelet adhesion is stabilized by another collagen receptor, integrin $\alpha_2\beta_1$ (31). Hence, the ability of CMPs to mimic collagen's biological function can be assessed by a platelet aggregation assay.

We examined 32-mer **1a–d**, type I collagen, 17-mer **2**, and 30-mer (POG)$_{10}$ (**4**) in various aggregation experiments with human platelets (Fig. 6 and Tables S2 and S3). Initially, solutions of the materials (2 mg/ml in PBS) except for collagen were incubated at 4°C for 7 days (Fig. 6*A*). Peptides **1a** and **1b**, and collagen, were potent platelet agonists with EC_{50} values of 4.1, 8.6, and 0.41 μg/ml, respectively; however, **1c** was a weak agonist, and **1d**, **2**, and **4** were inactive (Table S2). We wondered whether **4** might induce platelet aggregation after incubation under conditions of turbidity (see above). Thus, experiments were performed with **1a**, **1b**, and **4** incubated in PBS at 37°C for 80 min (7 mg/ml) or under the above conditions (2 mg/ml, 4°C, 7 days). In both cases, **4** was inactive, whereas **1a** and **1b** were potent agonists (EC_{50} = 1–2 μg/ml) in the realm of collagen (EC_{50} = 0.63 μg/ml) (Fig. 6*B* and Table S3). This result signifies that the aggregate from **4** is not collagen-like, in contrast to the self-assembled materials from **1a** or **1b**. Importantly, **1a** and **1b** were able to self-organize into bioactive materials at 37°C in a reasonable time frame of 80 min. Relative to thrombogenic pharmacology, preliminary studies with **1a** (in PBS for 7 days at 4°C) impregnated in a poly(ε-caprolactone-*co*-glycolide) foam exhibited topical hemostatic action in a porcine spleen-bleeding model (32, 33).

Discussion

We compared 32-mer peptides **1a–d** for their ability to mimic collagen structurally and functionally. Whereas **1a** and **1b** readily self-assembled into supramolecular, collagen-like materials, **1c** and **1d** did not. Peptides **1a** and **1b** had stable triple-helical character, formed micrometer-length fibrillar material, and were potent in inducing platelet aggregation.

The energetics for head-to-tail stacking of triple-helical homodimers of **1a–d** were explored via XED force-field calculations on 29-mer homologues **1a′–d′** with an optimal six-point model, involving three salt bridges and three aromatic interactions at the dimer interface. Energy-minimized (**1a′**)$_3$/(**1a′**)$_3$

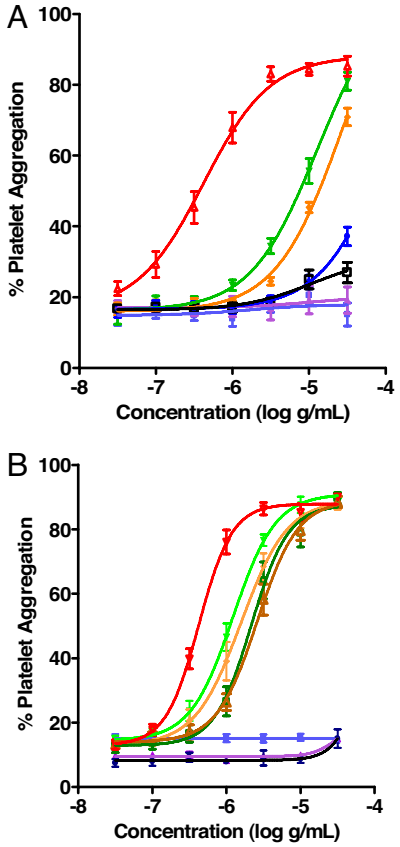

Fig. 6. Platelet aggregation experiments with peptides, under different conditions, and collagen. (*A*) **1a**, green; **1b**, yellow; **1c**, blue; **1d**, black; **2**, violet; **4**, light blue (2 mg/ml in PBS, incubated at 4°C for 7 days); and collagen, red. (*B*) **1a**, dark green; **1b**, yellow-brown; and **4**, black (7 mg/ml in PBS, incubated at 37°C for 80 min); **1a**, green; **1b**, yellow, diamond; **2**, violet; and **4**, blue (2 mg/ml in PBS, incubated at 4°C for 7 days); collagen (red, inverted triangle). EC_{50} values are given in Tables S2 and S3.

retained the six key interactions and had a total binding energy (*in vacuo*) of −83.5 kcal/mol, which is a 50% increase in stabilization energy relative to having just one salt bridge (22). In the final model (Fig. 2 and Fig. S1), the ion pairs are sheltered by the hydrophobic environment to contribute added stabilization. It is meaningful that the energies (kcal/mol) for the four triplex homodimers, which decreased in going from **1a**′ (−83.5) to **1b**′ (−70.4) to **1c**′ (−58.9) to **1d**′ (−43.8), trend with the platelet aggregation results for **1a–d** (EC_{50} potency: **1a**/**1b** ≫ **1c** > **1d**).

Our study of **1a–d**, structurally and biofunctionally, tested the self-assembly hypothesis by evaluating the importance of hydrophobic/ionic interactions in collagen mimicry. Peptide **1d** is an important example because it has an identical length to **1a–c** and can form three interfacial salt bridges but lacks hydrophobic end-groups. Peptides **1a–d** formed stable triple helices by CD with a narrow range of melting temperatures (T_m = 56–62°C), which signifies similar thermodynamic stability. These T_m values exceed that (T_m = 47°C) for a collagen-mimetic with three peptide strands covalently linked by disulfide bonds (14), but are lower than that (T_m = 70°C) for 31-mer $Ac(GPO)_{10}G$ (**3**) (22). By light microscopy, there was a clear difference between **1a** and **1d** in that **1a** formed fibrils but **1d** did not. Control peptide **4**, $(POG)_{10}$, which cannot capitalize on end-group hydrophobic or ionic interactions, self-associates and precipitates with increasing temperature and concentration (29). With aged solutions of **1a** and **4**, **4** formed a thick precipitate, but **1a** formed fine particles that appeared by light microscopy as a banded "worm-like" hydrogel (Fig. 5), consistent with an ordered, supramolecular material. For **1a**, we observed microfibrils by transmission EM (TEM) akin to collagen fibrils in murine aortic tissue (22). Given fibril dimensions of >1 μm long and 0.25 μm in diameter (22), triple-helical **1a** (9 nm long) associates by both linear (presumably head-to-tail) and lateral stacking, with >100 triple-helical building blocks in each direction. Thus, the aromatic end-groups facilitate both axial and lateral assembly.

The AFM topography images of **1a–d** displayed notably different morphologies. At 0.1 or 1.0 mg/ml **1a** and **1b** formed microfibrils, whereas **1c** and **1d** did not. In contrast, a collagen-mimetic with three peptide strands covalently linked by disulfide bonds, showed small, one-dimensional fibrils <120 nm in length by AFM (14). Clearly, this fibrillar material is very different from the long, three-dimensional fibrils obtained from **1a** and **1b**, which also exhibit periodicity (*D*) reminiscent of collagen. A recent report described a 36-mer peptide that self-assembles into banded collagen-mimetic fibrils driven by multiple electrostatic interactions (34).

Collagen can function as a signaling peptide (35), such as by interacting with cell-surface receptors GP VI and $\alpha_2\beta_1$ on platelets (30, 31). After damage to the blood vessel wall, exposed collagen induces platelets to adhere and aggregate. Synthetic triple-helical peptides containing the main collagen repeat, GPO (or analogues), offer useful tools to probe the structural basis of such platelet activation. For example, polymerization of short CMPs by chemical cross-linking led to materials that were highly platelet aggregatory (36), by direct action on GP VI (37). In a previous platelet aggregation study with solutions of **1a**, we used protracted incubation at 4°C to obtain an optimal effect (7 days in PBS; EC_{50} = 0.37 μg/ml) (22). Our present comparison of the thrombogenic properties of **1a–d**, 17-mer **2**, 30-mer $(POG)_{10}$ (**4**), and collagen with respect to human platelets (Fig. 6*A*) is informative. Peptides **1a** and **1b** were potent agonists, **1c** was a weak agonist, and **1d**, **2**, and **4** were inactive. In fact, robust platelet agonist activity was realized for **1a** and **1b** after brief incubation (80 min) at 37°C (Fig. 6*B*). Apparently, the Phe/Phe end-groups in **1b** are nearly as effective for facilitating self-assembly as the F_5-Phe/Phe end-groups in **1a**. Despite their hydrophobicity, Leu/Phe in **1c** is not a satisfactory arrangement. The failure of 17-mer **2**, with F_5-Phe/Phe end-groups, to induce platelet aggregation is due to its short sequence, which is inadequate for stable triple-helix formation. Because aggregation stimulated by **1a** was inhibited by the GP IIb/IIIa antagonist RWJ-53308 (38) dose-dependently (Fig. S8), **1a** acts via GP IIb/IIIa signaling (like collagen). Our AFM results, which depicted fibrillar species for **1a** and **1b**, but not for **1c** and **1d**, correlate with our platelet aggregation data. In summary, thrombogenesis required fibrous supramolecular structures; it was not caused by triple helical structures alone. As such, our study supports the fibrillar morphology of collagen as being critical for platelet binding and activation (36, 39, 40). The disparity in behavior between **1a**/**1b** and **1d**/**4** indicates the importance of hydrophobic aromatic interactions in the self-assembly of such triple-helical building blocks into collagen-like biomaterials.

In type I collagen, which has a 1,011-residue triple-helical section and telopeptide sequences at the N and C termini, the staggered assembly of five triple helices yields micrometer-length fibrils. There is characteristic banding in the superstructure from gaps in the ordered array of triple-helical bundles, with repeat spacing of 67 nm (28), corresponding to a cluster of conserved hydrophobic amino acids with a periodicity of 234 aa (41). Fibril assembly depends on the hydrophobic telopeptides, with their aromatic amino acids (F, Y) (20, 21), and fibril diameter is regulated by hydrophobic amino acids in the gap regions, via interaction with Leu-rich proteoglycans (42, 43). Our use of Leu in **1c** was connected with this point, but Leu also offered a nonaromatic hydrophobic

group to test the importance of aromatic-aromatic interactions. Clearly, the concept of hydrophobic self-assembly is intimately rooted in the structural characteristics of collagen. Our investigation extends this phenomenon to the spontaneous self-assembly of smaller peptide systems into fibrils. Specifically, short (9-nm) peptides **1a** and **1b** form triple helices that self-assemble into collagen-like fibrils with collagen-like biological properties. For archetype **1a**, we observed micrometer-length composite fibrils by TEM, light microscopy, and AFM; also, **1a** generated striated hydrogels of millimeter length. The comparative behavior of **1a** and **1b** vs. **1c**, **1d**, and **4** underscores the importance of hydrophobic aromatic interactions in the self-assembly process. This straightforward approach should provide a useful means to obtain collagen model peptides that can self-organize into fibrillar structures with biofunctionality.

Materials and Methods

General Experimental Information. Equine type-I collagen (92% identity to human collagen) was obtained from Chrono-Log. MALDI-TOF MS was performed with an Applied Biosystems Voyager-DE PRO Biospectrometry workstation linked to a delayed extraction laser-desorption mass spectrometer (α-cyano-4-hydroxycinnamic acid as matrix) at M-Scan. Amino acid analysis was performed with a Beckman 6300 Li-based analyzer (Molecular Structural Facility, University of California, Davis). Peptide **4** was purchased from Peptides International. Solutions were prepared based on peptide content with concentration established by the absorbance at 214 nm (PBS; $\varepsilon = 6.0 \times 10^4\ M^{-1}cm^{-1}$) or 215 nm (water; $\varepsilon = 6.5 \times 10^4\ M^{-1}cm^{-1}$). Peptide ultrafiltrations were done with Acrodisc syringe filters [0.45-μm poly(tetrafluoroethylene) membrane; Pall].

Peptide Synthesis and Purification. Materials for peptide synthesis are listed in the *SI Text*, *Peptides*. CMPs **1a–d** were prepared on an ABI 431 synthesizer by using FastMoc chemistry (0.1-mmol scale) with Fmoc-Phe-Wang (0.74 mmol/g, 100–200 mesh) or Fmoc-Gly-Wang (0.66 mmol/g, 100–200 mesh) resin beads (44, 45) and cleaved from the resin with CF_3CO_2H/(*i*-Pr)$_3$SiH/water (95:2.5:2.5; 2 h). Peptides were first purified by RP-HPLC at 60°C (*SI Text*, *Peptides*). Column heating was important to disaggregate the analytes and allow for efficient separation. Each peptide (white powder) was ≈85% pure by HPLC analysis and had a satisfactory amino acid analysis. MS values for **1a–d** were obtained by using MALDI-TOF MS $(M + Na)^+$, whereas ESI-MS was applied to **2**. Yields, peptide content, and MS data for **1a–d** and **2** are given in Table S4. These materials were used for CD, turbidity, and platelet aggregation experiments. Peptides **1a–d** were purified further by RP-HPLC at 65°C with mass-selective fractionation (*SI Text*, *Peptides*). For these refined samples of **1a–d**, molecular weights were confirmed by MALDI-TOF MS, and purities were assayed by analytical RP-HPLC at 65°C (*SI Text*, *Peptides*). Thus, we obtained **1a–d** with high purities of 95%, 93%, 98%, and 93%, respectively. These peptides were used for AFM and platelet aggregation studies. Similar aggregation results were obtained with both sets of peptides. The synthesis and purification of **2** was the same as that for **1a**; Ac(GPO)$_{10}$G, **3**, was prepared as described in ref. 22.

Circular Dichroism Spectroscopy. Solutions of **1a–d** and **2** (0.25 mM in water) were stored at 4°C for 24 h to permit triple-helix formation. CD spectra were recorded on an Aviv 215 spectrometer equipped with a Peltier temperature controller with 0.1-cm path-length quartz cells. The spectra were obtained at 25°C by signal-averaging four scans at a scan speed of 120 nm/min. CD melting curves for **1a–d** were obtained by monitoring the ellipticity at 225 nm from 20 to 100°C, at a rate of 1°C/min, with increments of 3°C and an equilibration time of 5 min. CD melting curves for **2** were obtained by monitoring the ellipticity at 222 nm from 5 to 60°C at a rate of 1°C/min, with increments of 2°C and an equilibration time of 5 min. Measured T_m (°C) values (± 2): **1a**, 56; **1b**, 57; **1c**, 59; **1d**, 62.

Turbidity Studies. Solutions of **1a** and **4** (5 mg/ml, PBS, pH 7.4) were heated at 80°C for 10 min and filtered (0.45 μm). The solutions were kept at 45°C for 90 min and the absorption at 313 nm was measured (Cary Eclipse spectrophotometer). The samples were aged at 23°C for 3 days. A large hydrated particle formed by **1a** was carefully deposited on a microscope slide and images were taken by using a Nikon stereoscopic zoom microscope (SMZ-U; 7.5×) equipped with a color CCD camera.

Computational Chemistry. A model for the triple helix of **1a** [(**1a**)$_3$] was constructed from the x-ray structure of 30-mer CMP (POG)$_4$(POA)(POG)$_5$ (PBD entry 1CAG) (46). The Ala was mutated to Gly, the C-terminal Gly was replaced by Phe (as in **1a**), and the N-terminal Pro-Hyp (PO) was replaced by F_5-Phe (as in **1a**). This 29-mer, **1a**′, as a triple-helix, (**1a**′)$_3$, was used for interface interaction studies (22). To relax strain, the (**1a**′)$_3$ model was energy minimized by using an OPLS-AA force field (47), with a generalized Born/surface area (GB/SA) water solvation model (Macromodel 9.0; Schrödinger). The C terminus of the triple helix was paired with the N terminus of another triple helix by alignment along the central axes to give (**1a**′)$_3$/(**1a**′)$_3$. The distances between the three ion pairs (salt bridges) and three centers of paired phenyls were monitored while manually adjusting the torsion angles for operative interactions in a six-point model. The portion of (**1a**′)$_3$/(**1a**′)$_3$ within 18 Å of the interface center was energy minimized with the SYBYL force field (SYBYL 7.3; Tripos). This minimized homodimer interface was used in place of the nonminimized interface and a new model was set up with the six key interactions. The entire (**1a**′)$_3$/(**1a**′)$_3$ ensemble was energy minimized with the XED force field (25, 26), which is able to predict aromatic stacking in accord with the experimental observations (23). Formal charges (ionized at pH 7) were set at 1/8th to compensate for charge attenuation by solvent, the dielectric constant was set at 2, and minimization was performed over all atoms of the homodimer ensemble (5,064 atoms) without any constraints to an exit rms limit of ≤0.01. The binding energy for the two triple helices was calculated by summing the pairwise coulombic and dispersive (van der Waals) interactions, including all intermolecular terms (but excluding intramolecular terms and energies between strands in the same 3-helix bundle) (*SI Text*, *Computational Work*). Starting models of **1b**′–**d**′, as triplex homodimers, were constructed from the **1a**′ starting model (before XED minimization) by suitably changing the end-groups. Homodimer ensembles of **1b**′–**d**′ were processed to obtain total binding energies. Dissection of binding energies into coulombic and dispersive terms revealed some interesting patterns, indicating that the most stable head-to-tail junction for **1a**′ forms without perturbing the favorable H-bond network (*SI Text*, *Computational Work*).

Atomic Force Microscopy. AFM imaging was performed with a confocal Raman-AFM alpha300 A,R (WITec Instruments) at 24 ± 2°C. For high-resolution imaging, the AFM was operated in AC-Mode with a damping of $r = 50\%$, with topography and phase images recorded simultaneously. The cantilevers (Nanoworld Arrow FMR) had a nominal spring constant of 2.8 N/m and resonance frequency of 70–80 kHz. Aqueous solutions of **1a–d** were heated to 73°C for 10 min, filtered (0.45 μm), diluted to 0.1 or 1.0 mg/ml, and let stand for 24 h at 23°C (molecular grade water). Equine type I collagen was used (0.1 mg/ml). Sample solutions (40 μl) were deposited on freshly cleaved mica (grade V-4; SPI Supplies) for 30–60 s, then gently rinsed with water and dried in air.

Platelet Aggregation. The ability of the **1a–d** to mimic collagen's biological function was evaluated in an aggregation assay with ''washed'' human platelets (*SI Text*, *Platelet Studies*). Platelet aggregation was initiated by addition of serial concentrations (0.01, 0.03, 0.1, 0.3, 1, 3, 10, 30 μg/ml) of equine type I collagen or test peptides dissolved in PBS (pH 7.4). The buffer served as a negative control. The 96-well assay plate was stirred constantly and intermittently placed in a microplate reader (Softmax; Molecular Devices) to measure optical density (650 nm) at 0 and 5 min after addition of the test solutions. Aggregation was calculated as the decrease in optical density between the measurements at t_0 and 5 min, and expressed as percentage of aggregation. For the first study, **1a–d**, **2**, and **4** were each dissolved in PBS at 2 mg/ml and each solution was incubated at 4°C for 7 days. In a second study, **1a**, **1b**, and **4** were each dissolved in PBS at 7 mg/ml and each solution was incubated at 37°C for 80 min; also, solutions of **1a**, **1b**, **2**, and **4** were reevaluated in the prior manner for comparison. Purchased collagen (1 mg/ml) was diluted into aggregation buffer. An experiment was conducted with GP IIb/IIIa antagonist RWJ-53308 (38) (*SI Text*, *Platelet Studies*).

ACKNOWLEDGMENTS. We thank Brett Tounge, Gregory Leo, Gyorgy Vas, Chunlin Yang, and Tom Parry for technical assistance and advice.

1. Khoshnoodi J, Cartailler J-P, Alvares K, Veis A, Hudson BG (2006) Molecular recognition in the assembly of collagens: Terminal noncollagenous domains are key recognition modules in the formation of triple helical protomers. *J Biol Chem* 281:38117–38121.
2. Carlier M-F, Pantaloni D (2007) Control of actin assembly dynamics in cell motility. *J Biol Chem* 282:23005–23009.
3. Binder WH, Smrzka OW (2006) Self-assembly of fibers and fibrils. *Angew Chem Int Ed* 45:7324–7328.
4. Laidman J, Forse GJ, Yeates TO (2006) Conformational change and assembly through edge β strands in transthyretin and other amyloid proteins. *Acc Chem Res* 39:576–583.
5. Ricard-Blum S, Ruggerio F, van der Rest M (2005) The collagen superfamily. *Top Curr Chem* 247:35–84.

6. Wess TJ (2005) Collagen fibril form and function. *Adv Protein Chem* 70:341–374.
7. Ramachandran GN, Kartha G (1955) Structure of collagen. *Nature* 176:593–595.
8. Rich A, Crick FHC (1961) The molar structure of collagen. *J Mol Biol* 3:483–506.
9. Holmgren SK, Taylor KM, Bretscher LE, Raines RT (1998) Code for collagen's stability deciphered. *Nature* 392:666–667.
10. Nishi Y, *et al.* (2005) Different effects of 4-hydroxyproline and 4-fluoroproline on the stability of collagen triple helix. *Biochemistry* 44:6034–6042.
11. Fields GB, Prockop DJ (1996) Perspectives on the synthesis and application of triple-helical, collagen-model peptides. *Biopolymers* 40:345–357.
12. Jenkins CL, Raines RT (2002) Insights on the conformational stability of collagen. *Nat Prod Rep* 19:49–59.
13. Koide T, Homma DL, Asada S, Kitagawa K (2005) Self-complementary peptides for the formation of collagen-like triple helical supramolecules. *Bioorg Med Chem Lett* 15:5230–5233.
14. Kotch F, Raines RT (2006) Self-assembly of synthetic collagen triple helices. *Proc Natl Acad Sci USA* 103:3028–3033.
15. Lehn J-M (2002) Toward self-organization and complex matter. *Science* 195:2400–2403.
16. McGaughey GB, Gagné M, Rappé AK (1998) π-Stacking interactions. *J Biol Chem* 273:15458–15463.
17. Oshovsky GV, Reinhoudt DN, Verboom W (2007) Supramolecular chemistry in water. *Angew Chem Int Ed* 46:2366–2393.
18. Ajayaghosh A, Praveen VK (2007) π-Organogels of self-assembled p-phenylenevinylenes: Soft materials with distinct size, shape, and functions. *Acc Chem Res* 40:644–656.
19. Reches M, Gazit E (2003) Casting metal nanowires within discrete self-assembled peptide nanotubes. *Science* 300:625–627.
20. Helseth DL, Jr, Veis A (1981) Collagen self-assembly in vitro. Differentiating specific telopeptide-dependent interactions using selective enzyme modification and the addition of free amino telopeptide. *J Biol Chem* 256:7118–7128.
21. Prockop DJ, Fertala A (1998) Inhibition of the self-assembly of collagen I into fibrils with synthetic peptides. Demonstration that assembly is driven by specific binding sites on the monomers. *J Biol Chem* 273:15598–15604.
22. Cejas MA, *et al.* (2007) Collagen-related peptides: Self-assembly of short, single strands into a functional biomaterial of micrometer scale. *J Am Chem Soc* 129:2202–2203.
23. Lozman OR, Bushby RJ, Vinter JG (2001) Complementary polytopic interactions (CPI) as revealed by molecular modelling using the XED force field. *J Chem Soc Perkin Trans* 2:1446–1453.
24. Gdaniec M, Jankowski W, Milewska MJ, Połoński T (2003) Supramolecular assemblies of hydrogen-bonded carboxylic acid dimers mediated by phenyl-pentafluorophenyl stacking interactions. *Angew Chem Int Ed* 42:3903–3906.
25. Vinter JG (1994) Extended electron distributions applied to the molecular mechanics of some intermolecular interactions. *J Comp-Aided Mol Design* 8:653–668.
26. Chessari G, *et al.* (2002) An evaluation of force-field treatments of aromatic interactions. *Chem–Eur J* 8:2860–2867.
27. Sakakibara S, *et al.* (1973) Synthesis of (Pro-Hyp-Gly)n of defined molecular weights. Evidence for the stabilization of collagen triple helix by hydroxypyroline. *Biochem Biophys Acta, Protein Struct* 303:198–202.
28. Baselt DR, Revel J-P, Baldeschwieler JD (1993) Subfibrillar structure of type I collagen observed by atomic force microscopy. *Biophys J* 65:2644–2655.
29. Kar K, *et al.* (2006) Self-association of collagen triple helix peptides into higher order structures. *J Biol Chem* 282:33283–33290.
30. Nieswandt B, Watson SP (2003) Platelet-collagen interaction: Is GPVI the central receptor? *Blood* 102:449–461.
31. Sarratt KL, *et al.* (2005) GPVI and $\alpha 2\beta 1$ play independent critical roles during platelet adhesion and aggregate formation to collagen under flow. *Blood* 106:1268–1277.
32. Yang C, *et al.* (2003) Development of a recombinant human collagen-type III based hemostat. *J Biomed Mater Res, Part B: Appl Biomater* 69B:18–24.
33. Cole DJ, *et al.* (1999) A pilot study evaluating the efficacy of a fully acetylated poly-*N*-acetyl glucosamine membrane formulation as a topical hemostatic agent. *Surgery* 126:510–517.
34. Rele S, *et al.* (2007) D-Periodic collagen-mimetic microfibers. *J Am Chem Soc* 129:14780–14787.
35. Leitinger B, Hohenester E (2007) Mammalian collagen receptors. *Matrix Biol* 26:146–155.
36. Morton LF, Hargreaves PG, Farndale RW, Young RD, Barnes MJ (1995) Integrin $\alpha 2\beta 1$-independent activation of platelets by simple collagen-like peptides: Collagen tertiary (triple-helical) and quaternary (polymeric) structures are sufficient alone for $\alpha 2\beta 1$-independent platelet reactivity. *Biochem J* 306:337–344.
37. Knight CG, *et al.* (1999) Collagen-platelet interaction: Gly-Pro-Hyp is uniquely specific for platelet Gp VI and mediates platelet activation by collagen. *Cardiovasc Res* 41:450–457.
38. Hoekstra WJ, *et al.* (1999) Potent, orally active GPIIb/IIIa antagonists containing a nipecotic acid subunit. Structure-activity studies leading to the discovery of RWJ-53308. *J Med Chem* 42:5254–5265.
39. Lecut C, *et al.* (2005) Fibrillar type I collagens enhance platelet-dependent thrombin generation via glycoprotein VI with direct support of $\alpha 2\beta 1$ but not $\alpha IIb\beta 3$ integrin. *Thromb Haemostasis* 94:107–114.
40. Savage B, Ginsberg MH, Ruggeri ZM (1999) Influence of fibrillar collagen structure on the mechanisms of platelet thrombus formation under flow. *Blood* 94:2704–2715.
41. Traub W (1978) Molecular assembly in collagen. *FEBS Lett* 92:114–120.
42. Iozzo RV (1997) The family of the small leucine-rich proteoglycans: Key regulators of matrix assembly and cellular growth. *Crit Rev Biochem Molec Biol* 32:141–174.
43. Chakravarti S, Zhang G, Chervoneva I, Roberts L, Birk DE (2006) Collagen fibril assembly during postnatal development and dysfunctional regulation in the lumican-deficient murine cornea. *Develop Dynam* 235:2493–2506.
44. White PD, Chan WC (2000) Basic principles of Fmoc solid-phase synthesis. In *Fmoc Solid-Phase Peptide Synthesis*, eds Chan WC, White PD (Oxford Univ Press, Oxford), pp 9–40.
45. Chan WC, White PD (2000) Basic procedures. In *Fmoc Solid-Phase Peptide Synthesis*, eds Chan WC, White PD (Oxford Univ Press, Oxford, UK), pp 41–76.
46. Bella J, Eaton M, Brodsky B, Berman HM (1994) Crystal and molecular structure of a collagen-like peptide at 1.9 Å resolution. *Science* 266:75–81.
47. Jorgensen WL, Tirado-Rives J (1988) The OPLS [optimized potentials for liquid simulations] potential functions for proteins, energy minimizations for crystals of cyclic peptides and crambin. *J Am Chem Soc* 110:1657–1666.